Micro-architectured materials: past, present and future

N. A. Fleck, V.S. Deshpande and M. F. Ashby

Cambridge University Engineering Dept.,
Trumpington St., Cambridge, CB2 1PZ, UK
Email: NAF1@eng.cam.ac.uk

Summary

Micro-architectured materials offer the opportunity of obtaining unique combinations of material properties. First, a historical perspective is given to the expansion of material property space by the introduction of new alloys and new microstructures. Principles of design of micro-architecture are then given and the role of nodal connectivity is emphasised for monoscale and multi-scale microstructures. The stiffness, strength and damage tolerance of lattice materials are reviewed and compared with those of fully dense solids. It is demonstrated that micro-architectured materials are able to occupy regions of material property space (such as high stiffness, strength and fracture toughness at low density) that were hitherto empty. Some challenges for the development of future materials are highlighted.

Submitted to Proc. Roy. Soc. A

20 April 2010

1. Introduction: a materials time-line

In this paper, the evolution of engineering materials is outlined, with the main enablers of change. The history of this evolution is illustrated in the first two sections of the paper, introducing the concept of *material property space*. Strategies are identified for filling the remaining gaps of this space. The ability of micro-architectured lattice materials to give a wide range of stiffness, strength and fracture toughness is described, with the role of nodal connectivity and structural hierarchy emphasised. The damage tolerance of lattice materials relative to that of the parent solid is then discussed, with an identification of several transition flaw sizes. Finally, some future directions are given for the future development of lattice materials and the utility of cross-property relations and bounding theorems is discussed.

Figure 1 is a materials time-line. It is interesting to follow its development, starting from the bottom and working upwards. The tools and weapons of prehistory, 300,000 or more years ago, were bone and stone. Stones could be shaped for tools, particularly flint and quartz, which can be flaked to produce a cutting edge that was harder, sharper more durable than any other material that could be found in nature. Gold, silver and copper, the only metals that occur in native form, must have been known from the earliest time, but the realization that they were ductile, could be beaten to complex shape, and – once beaten – became hard, seems to have occurred around 5500 BC. By 4000 BC there is evidence that technology to melt and cast these metals had developed, allowing more intricate shapes. Native copper, however, is not abundant. Copper occurs in far greater quantities as the minerals azurite and malachite. By 3500 BC, kiln furnaces, developed for pottery, could reach the temperature required for the reduction of these minerals, making copper sufficiently plentiful to be used for implements and weapons. But even in the worked state, copper is relatively soft. Around 3000 BC the accidental inclusion of a tin-based mineral, cassiterite, in the copper ores provided the next step in technology – the production of the alloy *bronze*, a mixture of tin and copper, with a strength and hardness that pure copper cannot match.

The discovery, around 1450 BC of ways to reduce ferrous oxides to make iron, a material with greater stiffness, strength and hardness than any other then available, rendered bronze obsolete. Iron was not entirely new: tiny quantities existed as the cores of meteors that had impacted the earth. The oxides of iron, by contrast, are widely available, particularly *hematite*, Fe_2O_3. Hematite is easily reduced by carbon, although it takes high temperatures, close to 1100 C, to do it. This temperature is insufficient to melt iron, so the material produced was a spongy mass of solid iron intermixed with slag; this was reheated and hammered to expel the slag and then forged into the desired shape. The casting of iron was a more difficult challenge, requiring temperatures of around 1600 C. Two millennia passed before, in 1500 AD, the blast furnace was developed, enabling the widespread use of cast iron. Cast iron allowed structures of a new type: the great bridges, railway terminals and civil building of the early 19th century are testimony to it. But it was steel, made possible in industrial quantities by the Bessemer process of 1856, that gave iron its dominant role in structural design that it still holds today.

The demands of the expanding aircraft industry in the 1950s shifted emphasis to the light alloys (those of aluminum, magnesium and titanium) and to materials that could withstand the extreme temperatures of the turbine combustion chamber. The development of superalloys – heavily alloyed iron, nickel and cobalt-based materials – became the focus of research, delivering an extraordinary range of alloys able to carry load at temperatures above 1200 C. The range of their applications expanded into other fields particularly those of chemical and petroleum engineering.

The history of polymers is rather different. Wood, of course, is a polymeric composite, one used for construction from the earliest times. The beauty of amber – petrified resin – and of horn and tortoise shell – the polymer *keratin* – already attracted designers from the earliest times. Rubber, brought to the Europe in 1550, grew in importance in the 19th century, partly because of the wide spectrum of properties made possible by vulcanization – cross-linking by sulphur – giving materials as elastic as latex or as rigid as ebonite. The real polymer revolution, however, has its beginnings in the early 20th century with the development of Bakelite, a phenolic, in 1909 and synthetic butyl rubber in 1922. This was followed in mid-century, by a period of rapid development of polymer science. Almost all the

polymers we use so widely today were developed in a 20 year span from 1940 to 1960, among them the bulk commodity polymers polypropylene (PP), polyethylene (PE), polyvinyl chloride (PVC) and polyurethane (PU), the combined annual tonnage of which now approaches that of steel. Design with polymers has matured: they are now as important as metals in household products, automobiles, and, most recently, in aerospace. Unreinforced polymers lack the stiffness and strength many of these applications demand. They are used, instead, as *composites*, reinforced with fillers and fibres. Composite technology is not new. Straw-reinforced mud brick is one of the earliest of the materials of architecture and remains one of the traditional materials for building in parts of Africa and Asia even today. Steel-reinforced concrete – the material of shopping-centres, road bridges and apartment blocks – appeared just before 1850. The reinforcement of polymers was enabled by the technology for making glass fibres, which had existed since 1880. Glass wool, or better, woven or layered glass fibres, could be incorporated in thermosetting polyesters or epoxies, giving them the stiffness and strength of aluminum alloys. By the mid 1940s glass fibre reinforced polymer (GFRP) components were in use in the aircraft industry. The real transformation of polymers into high performance structural materials came with the development of aramid and carbon fibres in the 1960s. Incorporated as reinforcements, they give materials with performance (meaning stiffness and strength per unit weight) that exceeded that of all other bulk materials, giving them their now-dominant position in high-performance sports equipment and aerospace.

The period in which we now live might have been named the polymers and composites-era had it not coincided with a second revolution, that based on silicon. Silicon was first identified as an element in 1823, but found few uses until the discovery, in 1947, that, when doped with tiny levels of impurity, it could act as a rectifier. The discovery has created the fields of electronics, mechatronics and modern computer science, revolutionizing information storage, access and transmission, imaging, sensing and actuation, numerical modeling and much more. This is rightly called the information age, enabled by the development of transistor-grade silicon.

In the last two decade, the areas of biomaterials has developed rapidly. Implanting materials in or on the human body was not practical until aseptic surgical technique

was developed in the late 1800's. Non-toxic metal alloys were introduced but tended to fracture in service. It was not until the development of polymer-based systems, and subsequently, with a new wave of discoveries in cell biology, chemistry, and materials science, that synthetic biomaterials became a reality.

During the early 90s it was realized that material behaviour depended on scale, and that the dependence was most evident when the scale was that of nanometers. Although the term nano-science is new, the use of nano-technology is not. The proteins and minerals of soft and mineralized tissue in plants and animals are dispersed on a nano-scale. Nanoparticles of carbon have been used for the reinforcement of tires. The light alloys of aerospace are derive their strength from a nano-scale dispersion of precipitates. Modern nano-technology gained prominence with the discovery of various forms of carbon such as the C60 molecule and carbon nano-tubes, though even these are not really new but have always existed as particles in smoke. True nano-engineering has finally come with the development of tools capable of resolving and manipulating matter at the atomic level, making it possible (though at present expensive) to build materials and structures the way nature does it, atom by atom and molecule by molecule.

Figure 1 tracks the expanding portfolio of materials available to the engineer. With it comes an expansion of the accessible range of stiffness, strength and toughness. The expansion of one of these – strength – is illustrated in the next section.

2. Expanding the boundaries of material-property space

The material development documented in the time-line were driven by the desire for ever greater performance. One way of examining the progress of this is by following the way in which properties have evolved on *material property charts.* Material property charts (Ashby, 2010) display materials on axes based on two of their properties. Materials have many properties of course – mechanical, thermal, electrical, optical and many more – so the number of such pair-wise combinations is large. Each chart can be thought of as a slice through "material property space" – a multidimensional space with material properties as its axes.

Figure 2 is an example of just one of them. It is a *Strength-Density chart*. There are many obvious incentives for seeking materials with greater strength: more durable and effective tools and weapons; faster, more economical transport; larger, more daring structures. In more recent times it has been high strength at low weight that is frequently sought, with transport and aerospace as the direct drivers.

The chart is plotted for six successive points in historical time, ending with the present day. The materials of pre-history, shown at (a), cover only a tiny fraction of this strength-density space. By the time of the peak of the Roman empire, around 50 BC (b), the area occupied by metals has expanded considerably. The progress thereafter was slow: 1500 years later (c) not much has changed, although, significantly, cast iron now appears. Even 500 years after that (d) expansion of the occupied area of the chart is small; aluminium only just creeps in. Then things accelerate. By 1945 the metals envelope has expanded considerably and a new envelope – that of synthetic polymers – now occupies a significant position. Between then and the present day the expansion has been dramatic. How much further can we go? That is a question we explore in the sections that follow.

3. Strategies for filling material property space

Material property charts each have the feature that parts of them are populated with materials and parts are not – there are holes. Some parts are inaccessible for fundamental reasons that relate to the size of atoms and the nature of the forces that bind them together. But other parts are empty even though, in principle, they are could be filled.

One approach to filling holes in material property space is that of manipulating *chemistry*, developing new metal alloys, new polymer formulations and new compositions of glass and ceramic that extend the populated areas of the property charts. A second is that of manipulating *microstructure*, using thermo-mechanical processing to control the distribution of phases and defects within materials. Both have been exploited systematically, leaving little room for further gains, which tend to be incremental rather than step-like. A third approach is that of controlling

architecture to create hybrid materials – combinations of materials or of material and space in configurations and with connectivities that offer enhanced performance. The success of carbon and glass-fibre reinforced composites at one extreme, and of foamed materials at another in filling previously empty areas of the property charts is encouragement enough to explore this route in greater depth. In the present study, we limit attention to the extreme case of porous solids (a hybrid of the solid and air), and explore the effect of micro-architecture upon properties.

Lattice materials

We define a general *lattice material* as a cellular, reticulated, truss or lattice structure made up of a large number of uniform lattice elements (e.g. slender beams or rods) and generated by tesselating a unit cell, comprised of just a few lattice elements, throughout space. Here we use the term "material" to emphasise that we shall consider lattice structures with global, macroscopic length scales much larger than that characteristic of their constituent lattice elements (e.g. individual rod length).

Classically, periodic *planar lattices* are classified as *regular*, *semi-regular* or other. *Regular lattices* are generated by tesselating a regular polygon to fill the entire plane (Cundy & Rolett, 1961; Frederickson, 1997; Lockwood & Macmillan, 1978). Only a few regular polygons produce such a lattice: these are the triangle, square and hexagon with sketches of the triangulated and hexagonal lattice included in Fig. 3. *Semi-regular lattices* are generated by tesselating two or more different kinds of regular polygons to fill the entire plane (Cundy & Rolett, 1961; Frederickson, 1997; Lockwood & Macmillan, 1978). It may be shown that there only eight, independent, such lattices and no more. An example of such a lattice is the "triangular-hexagonal" lattice, also known as the *Kagome* lattice (Hyun & Torquato, 2002; Syozi, 1972). Additional plane-filling lattices can be constructed from two or more polygons of different size, or by relaxing the restriction that each joint has the same connectivity, see for example Hutchinson (2004).

Spatial or 3D lattices can be generated by filling space from polyhedra. Of the regular polyhedra with a small number of faces only the cube and the rhombic dodecahedra can be tesselated to fill all space (Gibson and Ashby, 1997). Typically spatial lattices

are constructed using combinations of different: for example, tetrahedra and octahedra may be packed to form the octet-truss lattice (Deshpande et al., 2001).

In the following we shall argue that the properties of lattice materials are dictated by the volume fraction of cell wall material and also by the nodal connectivity: the number of struts that meet at each node of the microstructure.

4. Expanding property space by the design of lattice materials

The relative density $\bar{\rho}$ of a lattice material is defined as the ratio of the density of the lattice material to the density of the solid. Lattice materials resemble frameworks when $\bar{\rho}$ is less than about 0.2, and in this regime $\bar{\rho}$ is directly related to the thickness *t* and length ℓ of a strut according to

$$\bar{\rho} = A\left(\frac{t}{\ell}\right) \qquad (1)$$

for a 2D lattice. The constant of proportionality *A* depends upon the geometry: for the hexagonal, Kagome and fully triangulated lattices as shown in Fig. 3 we find that *A* equals $2/\sqrt{3}$, $\sqrt{3}$ and $2\sqrt{3}$ respectively, as listed in Table 1.

Table 1. Coefficients for the scaling laws

Topology	*A*	*B*	*b*	*v*	*C*	c	*D*	*d*
Hexagonal	$2/\sqrt{3}$	3/2	3	1	1/3	2	0.90	2
Triangular	$2\sqrt{3}$	1/3	1	1/3	1/3	1	0.61	1
Kagome	$\sqrt{3}$	1/3	1	1/3	1/2	1	0.21	1/2

A 3D lattice or foam can be either open or closed celled, as follows. *Open-celled* microstructures comprise a 3D arrangement of inter-connected struts, and have the property that $\bar{\rho}$ scales with $(t/\ell)^2$. *Closed-cell* microstructures also exist, with plate-like cell faces of thickness *t* and side length ℓ; their relative density scales with (t/ℓ) provided the cell faces have uniform thickness. Closed cell foams, typically, have thickened cell edges; giving a dependence of $\bar{\rho}$ on (t/ℓ) between these two extremes.

The role of nodal connectivity

There are two distinct species of cellular solid. The distinction is most obvious in their mechanical properties. The first, typified by foams, are *bending-dominated structures*; the second, typified by triangulated lattice structures, are *stretching-dominated* – a distinction explained more fully below, and detailed in Deshpande et al. (2001b). To give an idea of the difference: a foam with a relative density of 0.1 (meaning that the solid cell walls occupy 10% of the volume) is less stiff by a factor of 3 than a triangulated lattice of the same relative density. The macroscopic properties are largely dictated by the connectivity of joints rather than by the regularity of the microstructure.

The distinction of a bending-dominated structure and a stretching-dominated microstructure structure is closely linked to the collapse response of a pin-jointed structure of the same morphology. If the parent, pin-jointed lattice exhibits collapse mechanisms that generate macroscopic strain, then the welded-joint version relies upon the rotational stiffness and strength of the nodes and struts for its macroscopic behaviour: consequently, the parent lattice is bending-dominated. In contrast, when the parent lattice has only periodic collapse mechanisms or no collapse mechanisms, the welded-joint version is stretching-governed. In broad terms the type of response is dependent upon the nodal connectivity.

Maxwell analysed a pin-jointed frame (meaning one that is hinged at its corners) made up of b struts and j frictionless joints, like those in Fig. 3. He showed that a 2D *statically* and *kinematically determinate* frame (one that is just rigid and does not fold up when loaded) has the property that

$$b - 2j + 3 = 0 \tag{2}$$

In 3-dimensions the equivalent equation is

$$b - 3j + 6 = 0 \tag{3}$$

A generalisation of the Maxwell rule in 3D is given by Calladine (1978) as

$$b - 3j + 6 = s - m \qquad (4)$$

where s and m count the states of self stress and mechanisms, respectively, and each can be determined by finding the rank of the equilibrium matrix that describes the frame in a full structural analysis (Pellegrino and Calladine, 1986). A just rigid framework (i.e. a framework that is both statically and kinematically determinate) has $s=m=0$. The nature of Maxwell's rule as a necessary rather than sufficient condition is made clear by examination of Eq. (2): vanishing of the LHS in Eq. (2) only implies that the number of mechanisms and states of self-stress are equal, not that each equals zero. If $m > 0$, the frame contains *mechanisms*. It has no stiffness or strength; it collapses if loaded. If its joints are locked, preventing rotation (as they are in a lattice) the bars of the frame *bend*. If, instead, $m = 0$ the frame ceases to be a mechanism. If it is loaded, its members carry tension or compression (even when pin-jointed), and it becomes a *stretch-dominated* structure. Locking the hinges now makes little difference because slender structures are much stiffer when stretched than when bent.

We now turn our attention to a large pin-jointed framework of connectivity Z and j joints: the total number of bars b is approximately $jZ/2$. The necessary, but not sufficient, condition for rigidity is $Z = 4$ in 2D and $Z = 6$ in 3D (Deshpande et al. 2001). A Venn diagram to illustrate the various types of mechanism exhibited by classes of 2D periodic pin-jointed truss is given in Fig. 4. Consider the various structures in turn. The fully triangulated structure, comprising equilateral triangles with a nodal connectivity of $Z = 6$, is highly redundant and possesses no collapse mechanisms. In contrast, a triangular-triangular lattice, with unit cell shown in Fig. 4, collapses by a mechanism which leads to a macroscopic hydrostatic strain. Thus, this structure has zero macroscopic stiffness against this collapse mode. The Kagome microstructure has a connectivity of $Z = 4$ and has no strain-producing collapse mechanisms; it can only collapse by periodic mechanisms which do not produce a macroscopic strain. Consequently, it is rigid in all directions. The cases of the square lattice and the hexagonal lattice, with a connectivity of $Z = 4$ and $Z = 3$, respectively, are different. Each of these structures can collapse by macroscopic strain-producing

mechanisms, and by periodic collapse mechanisms. A methodology has been developed by Hutchinson and Fleck (2005) to explore the periodic collapse mechanisms based on Bloch-wave analysis; the details are beyond the scope of the present article. The main conclusion to draw from Fig. 4 is that the fully triangulated structure is macroscopically stiff because it possesses no collapse mechanisms while the Kagome structure is macroscopically stiff because it has only periodic collapse mechanisms which generate no macroscopic strain.

The in-plane stiffness of 2D isotropic lattice materials

Material property space can be expanded by suitable design of material architecture. To illustrate this, consider the in-plane properties of 2D isotropic lattice materials: the hexagonal, Kagome and triangular lattices of nodal connectivity 3, 4 and 6, respectively, as sketched in Fig.3. We begin by reviewing briefly the macroscopic in-plane stiffness of these 2D lattices. Simple beam theory can be used to determine the effective, macroscopic Young's modulus E and Poisson ratio ν of the lattices in terms of the relative density $\bar{\rho}$. The scaling law can be adequately represented by the power-law expression,

$$\frac{E}{E_s} = B\bar{\rho}^b \tag{5}$$

where the values of the coefficient B and exponent b are listed in Table 1. The Poisson ratio ν is independent of relative density, assuming it is sufficiently low for beam theory to be adequate in characterising the behaviour of the lattice material. But ν does depend upon geometry, as summarised in Table 1. The hexagonal lattice is bending-dominated, with b=3. In contrast, the Kagome and fully triangulated lattices are stretching-dominated with b=1. Remarkably, the coefficient B and the Poisson ratio are also identical for the triangulated and Kagome lattices: these lattice have identical effective properties, and each achieves the Hashin-Shtrikhman upper bound. The differences between the two lattice do show up however when imperfections are introduced. For example, by randomly perturbing the location of the nodes at fixed relative density there is a large drop in the modulus of the Kagome lattice but a much smaller drop in modulus of the triangulated lattice (Romijn and Fleck (2007)). This is due to the fact that the triangulated lattice has a higher nodal connectivity of Z=6 than that of the Kagome lattice (Z=4) and is a much more redundant structure when the

struts are assumed to be pin-jointed at the nodes. The role of imperfection for these two lattices is further explored below for the property of fracture toughness.

The strength of 2D lattice materials

Beam theory can also be used to determine the macroscopic fracture strength of the perfect lattice, in the absence of heterogeneities such as a macroscopic crack. Consider the lattices of Fig. 3 loaded macroscopically by a uniform in-plane stress. The lattice responds in a linear-elastic manner, with a stress state within each bar given by simple beam theory. Define failure of the lattice as the point at which the maximum local tensile stress within the lattice attains the tensile fracture strength of the solid σ_{TS}. The corresponding macroscopic stress defines the fracture strength of the lattice. None of the three lattices of Fig. 3 possess an isotropic fracture strength – the macroscopic tensile strength of the lattice varies with the direction of loading. However, Gibson and Ashby (1997) have shown that the degree of anisotropy is small. For definiteness, we review here the macroscopic uniaxial strength σ_c of the lattice, upon loading along the x_2 direction as shown in Fig. 3. The strength σ_c can be expressed in terms of the tensile fracture strength of the solid, as

$$\frac{\sigma_c}{\sigma_{TS}} = C\bar{\rho}^c \tag{6}$$

with the coefficients (C, c) dependent upon geometry as listed in Table 1. The triangular and Kagome structures deform by bar stretching, and this leads to c=1, while the hexagonal honeycomb deforms by bar bending, giving c=2.

3D lattices and foams

Now consider the case of open-cell metallic foams, as reviewed by Ashby et al. (2000). They are manufactured mostly from the melt by the expansion of gas bubbles, and the expansion process is driven by the minimisation of surface energy. Consequently, they have microstructures which, although stochastic, have a low nodal connectivity of 3 – 4 adjoining bars per joint. The stiffness and strength of these 3D structures relies upon the bending stiffness of the bars, and they are consequently referred to as *bending-dominated structures*. It follows from beam-bending theory and dimensional analysis that the Young's modulus E of open-cell foams scales with that

of the fully dense solid E_S according to $E \approx \bar{\rho}^2 E_S$. The yield strength σ_Y scales with $\bar{\rho}$ and with the yield strength of the parent solid σ_{YS} according to $\sigma_Y \approx 0.3\bar{\rho}^{3/2}\sigma_{YS}$. Both relations are supported by a wealth of experimental data, see Ashby et al. (2000). In contrast, the octet truss, identical in crystal structure to face-cenetred cubic, has a nodal connectivity (co-ordination number) of 12 and is a *stretching-dominated structure*. Stretching-dominated microstructures have the property that their Young's modulus *E* and their yield strength σ_Y scale linearly with relative density $\bar{\rho}$ such that $E \approx 0.3\bar{\rho}E_S$ and $\sigma_Y \approx 0.3\bar{\rho}\sigma_{YS}$. (These values are on the order of the Hashin- Shtrikhman upper bound for an isotropic solid.) Such lattice materials have the virtue that the stiffness and strength scale linearly with the relative density and thereby out-perform metallic foams. A variety of fabrication routes have evolved to construct these periodic lattices, see Wadley et al. (2003).

It is instructive to display bending-dominated foams and stretching-dominated lattice materials in property space using the axes of *E* versus density and σ_Y versus density, see Fig. 5. The properties of the lattice materials scale linearly with density from that of the parent material, and fill-in some of the gaps of material property space. In contrast, the stiffness and strength of foams degrade at a faster rate than linearly with a decrease in density.

5. Multiscale lattice materials

Nature makes use of *multiscale* lattice materials, such that the material within each strut of the lattice comprising a lattice on a successively smaller scale (Ashby, 1991, 2010). One reason for such structural hierarchy in engineering structures is to increase buckling strength: recall that the buckling strength scales with any representative strut length ℓ according to ℓ^{-2}, and so the finer the length scale the higher the buckling strength.

Nature frequently designs *compliant structures* which have sufficiently low modulus that low stresses are generated upon deformation, and the structures do not fail. Soft tissue is of this type: skin, cartilage, and elastin along with many types of bird's nests

such as the woven Weaver bird's nest. One way of achieving low stiffness is to use structural hierarchy with a bending-dominated structure on various length scales.

Consider as a prototypical example a lattice material with struts (labelled 1) on a large scale made in turn from another lattice material with struts on a fine scale (labelled 2), as sketched in Fig. 6. The effective modulus E_2 of the fine-scale struts scales with the modulus E_S and relative density of the fine scale struts $\bar{\rho}_2$ according to

$$E_2 = B_2 \bar{\rho}_2^{b_2} E_S \tag{7}$$

Now construct the larger scale lattice material such that its struts are made from the fine-scale lattice of E_2. With the volume fraction of strut material 2 in the lattice material 1 written as $\bar{\rho}_1$ we note that the relative density of lattice material 1 to the solid is $\bar{\rho} = \bar{\rho}_1 \bar{\rho}_2$. Also, the effective modulus of the coarse-scale lattice E_1 is

$$E_1 = B_1 \bar{\rho}_1^{b_1} E_2 = B_1 B_2 \bar{\rho}_1^{b_1} \bar{\rho}_2^{b_2} E_S \tag{8}$$

and for the case $b_1 = b_2$ this simplifies to

$$E_1 = B_1 B_2 \bar{\rho}^{b_1} E_S \tag{9}$$

Now consider some examples from Nature where the large-scale lattice 1 is a bending or stretching structure and the finer-scale lattice 2 (making up the struts of the larger lattice) is a bending or stretching structure. We consider each case in turn.

Case I: a stretching-stretching structure

When both lattices have sufficient nodal connectivity that they are stretching-dominated in behaviour, we have $b_1 = b_2 = 1$ and the overall modulus E_1 is high. An example of this is the axial stiffness of woods: the cell walls are arranged as hexagonal prisms and along the prismatic direction the macro-lattice undergoes plate-stretching.

On a finer scale, each cell wall contains long fibres of cellulose and these too undergo stretching.

Case II: a bending-bending structure

Highly compliant lattices can be made by exploiting bending of the primary struts of the lattice, along with the use of compliant cell wall material (bending-dominated deformation of the finer-scale lattice). For an open-cell foam-like structure on both lengths scales we have $b_1 = b_2 = 2$. Consider as an example, birds nests that have been made by weaving together the leaves of grass. The grass leaves are wavy and bend when the nest is deformed. And on a finer scale the grass is composed of a 3D foam-like arrangement of cells with wavy sides. At this structural level too the cell walls bend under an imposed straining of the grass leaf. Consequently, the nest has a very low effective modulus. This is useful in making the nest damage tolerant during tropical storms.

Case III: a stretching-bending structure

The intermediate case is a stretching-dominated lattice on one length scale and a bending dominated lattice on a finer (or coarser scale) is also present in nature. Consider first the example of the transverse modulus of wood. On a coarse scale the microstructure comprises a 2D hexagonal lattice of wood cells, and the transverse modulus is dictated by bending of the cell walls, giving $b_1 = 3$. Bending of the cell walls involves stretching of the cellulose fibres within each cell wall, implying that $b_2 = 1$, and so the overall effective modulus is a result of bending on the coarse scale and stretching on the fine scale.

Second, consider a bird's wing which comprises a sandwich panel with solid faces and core struts. On the coarse scale, the struts undergo stretching ($b_1 = 1$), while on a finer scale they comprise a 3D foam-like microstructure that undergoes bending $(b_2 = 2)$. The spectrin-based cytoskeleton on the cytosolic side of the human red blood cell membrane is another example of a stretching-bending structure. On the coarse scale the spectrin is a fully triangulated, stretching-dominated lattice covering the cell membrane whereas the spectrin fibres are elastomeric with a low modulus.

6. The fracture toughness of lattice materials

The fracture toughness of lattice materials can be calculated upon assuming that the individual struts behave as elastic-brittle beams and fail when the maximum local tensile stress at any point in the lattice attains the solid strength σ_f. Consider a finite lattice domain surrounding the tip of a macroscopic crack (see Fig. 7). The displacements $\boldsymbol{u}$ and material rotation ψ of the beam ends are prescribed on the outer boundary according to the asymptotic *K*-field of a crack in an equivalent homogenous material possessing the effective elastic properties. The fracture toughness of the lattice is the value of applied stress intensity factor *K* that such that the maximum local tensile stress attains the value σ_f. This formulation, referred to as a boundary layer analysis, was first employed by Schmidt and Fleck (2001) to investigate crack growth initiation and subsequent propagation for regular and irregular elastic-plastic hexagonal lattices.

Fleck and Qiu (2006) have determined the fracture response of three elastic-brittle, isotropic lattices: hexagonal, triangular, and Kagome (Fig. 3). They found that the fracture toughness K_{IC} of these lattices scales with relative density $\bar{\rho}$ according to

$$\frac{K_{IC}}{\sigma_{TS}\sqrt{\ell}} = D\bar{\rho}^{d} \tag{10}$$

where the exponent d equals 2 for the hexagonal lattice, equals unity for the triangular lattice, and equals 0.5 for the Kagome lattice, see Table 1.

It is emphasised that the value of the exponent *d* gives the sensitivity of fracture toughness to relative density. For example, at a relative density of 10%, the fracture toughness of the Kagome lattice is 10 times greater than that of the hexagonal lattice (see Fig. 5). The unusually high fracture toughness of the Kagome lattice is attributed to the presence of an elastic zone of bending emanating from the crack tip into a remote stretching field. The Kagome lattice exhibits pronounced crack tip blunting due to the deformation band at the crack tip; this elastic blunting phenomenon reduces the stress levels at the crack tip and thereby increases the fracture toughness. Quintana-Alonso and Fleck (2009) found a similar effect for the diamond-celled lattice. A

particular feature of the diamond lattice is a low resistance to shear along the $\pm 45^{o}$ directions; the elastic bending zones emanate from the crack tip along these directions.

We proceed to relate the fracture toughness K_{IC} of a lattice to the fracture toughness K_{IC}^{S} of the cell wall material. Assume that the fracture strength σ_{TS} of the cell wall of a lattice material is dictated by the fracture toughness of the cell wall K_{IC}^{S} via an intrinsic flaw size a_0, according to

$$\sigma_{TS} = \frac{K_{IC}^{S}}{\sqrt{\pi a_0}} \tag{11}$$

Now substitute into (10) to obtain:

$$\frac{K_{IC}}{K_{IC}^{S}} = D\bar{\rho}^{d}\left(\frac{\ell}{\pi a_0}\right)^{1/2} \tag{12}$$

This expression is valid at low relative density. At high relative density, a more accurate expression would be

$$\frac{K_{IC}}{K_{IC}^{S}} = \bar{\rho} \tag{13}$$

In order to obtain a single expression that attains both asymptotes we introduce an arbitrary weight function $w(\bar{\rho})$ where

$$w(\bar{\rho}) = \exp\left(-\frac{\bar{\rho}}{(1-\bar{\rho})\bar{\rho}_0}\right) \tag{14}$$

The parameter $\bar{\rho}_0$ can be interpreted to be the value of relative density at which the fracture toughness switches from the dilute lattice limit to that of a solid containing a dilute concentration of voids. Upon combining (12-14) we obtain

$$\frac{K_{IC}}{K_{IC}^{S}} = w(\bar{\rho})D\bar{\rho}^{d}\left(\frac{\ell}{\pi a_0}\right)^{1/2} + (1 - w(\bar{\rho}))\bar{\rho} \tag{15}$$

The relation (15) is plotted in Fig. 9 for three representative choices of the ratio ℓ / a_0 and the transition relative density $\bar{\rho}_0 = 0.3$. For high values of ℓ / a_0, the fracture toughness of the lattice can be comparable to that of the parent solid material even though the effective density of the lattice is 100 times less than the parent solid. This is primarily due to the discreteness of the lattice, i.e. the stress field deviates from the *K*-field solution at a distance on the order of ℓ from the crack tip resulting in the enhanced fracture toughness. Figure 10 is a Fracture toughness – Density chart onto which this equation has been plotted for a Kagome lattice made of zirconia, ZrO_2. It uses values for (*D*, *d*) from Table 1, the values $K_{IC}^{S} = 7\text{MPa}\sqrt{\text{m}}$ and $\rho_S = 6000\,\text{kgm}^{-3}$ describing fully dense zirconia, and the parameter values $\ell / a_o = 1000$ and $\bar{\rho}_o = 0.3$. It illustrates the potential that architectured materials, particularly those with the Kagome architecture, have for enabling the toughening of brittle materials.

The Kagome lattice has a remarkably high fracture toughness, such that K_{IC} scales with $\bar{\rho}^{1/2}$ for $\bar{\rho} << 1$. Upon recalling that the effective Young's modulus of the lattice scales as $\bar{\rho}$ it follows that the toughness $G_{IC} = \left(1-\nu^2\right)K_{IC}^2 / E$ of the lattice is independent of relative density. This is a remarkable result. But now a word of caution. All this is for the perfect lattice. Romijn and Fleck (2007) have shown that K_{IC} (and *E*) are imperfection-sensitive for the Kagome lattice.

7. The damage tolerance of lattice materials

When a lattice material contains a short crack, its tensile strength is dictated by the tensile fracture strength of the lattice material σ_c. In contrast, when the lattice material contains a sufficiently long internal crack of length $2a$, its tensile strength is of order

$$\sigma = \frac{K_{IC}}{\sqrt{\pi a}} \tag{16}$$

in terms of the fracture toughness K_{IC} of the lattice material. A *transition flaw size* a_T can be identified immediately, of magnitude

$$a_T = \frac{1}{\pi}\left(\frac{K_{IC}}{\sigma_c}\right)^2 = \frac{1}{\pi}\left(\frac{D}{C}\right)^2 \bar{\rho}^{2(d-c)}\ell \qquad (17)$$

upon making use of (6) and (10). Then, for a less than a_T, the lattice material is flaw-insensitive and has a tensile strength close to σ_c whereas for a greater than a_T, the tensile strength is dictated by the fracture toughness of lattice, see Fig. 11.

It is instructive to compare the defect tolerance of an elastic-brittle lattice with that of the solid. Suppose the solid contains an internal crack of length 2a. The dependence of tensile strength of the solid upon a is included in Fig. 11. For a less than the intrinsic flaw size a_0, the tensile strength is given by $\sigma_{TS} = K_{IC}^S / \sqrt{\pi a_0}$, while for $a > a_0$ the tensile strength is given by $\sigma_{TS} = K_{IC}^S / \sqrt{\pi a}$. Consequently, a_0 serves the role of the transition flaw size for the solid.

We further note from Fig. 11 that the tensile strength of the defective lattice *exceeds* that of the parent solid provided the flaw size a is greater than a transition value

$$a_L = \frac{1}{\pi}\left(\frac{K_{IC}^S}{\sigma_C}\right)^2 = C^{-2}\bar{\rho}^{-2c}a_0 \qquad (18)$$

via (6) and (11). Thus, for a triangulated lattice (c=1) of relative density $\bar{\rho} = 3\%$ and $C \approx 1$, we find that $a_L = 1000a_0$. Typically, for ceramics, the intrinsic flaw size is on the order of 10 μm, and so a_L is on the order of 10mm. Thus, lattice materials compete with the parent solid in terms of damage tolerance for practical designs where flaws exist on the centimetre length scale. It is noteworthy that the transition flaw size a_L is sensitive to the relative density of the lattice but not to the cell size ℓ.

8. Future directions

Lattice materials show promise for multifunctional applications, combining a mechanical function (such as stiffness and strength) with some other property (such as thermal or electrical conductivity), thereby making structural batteries, structural armour and deployable materials a possibility. Recently, it has been recognised that lattice materials have a morphing capability provided the parent pin-jointed lattice is statically and kinematically determinate, see for example Hutchinson and Fleck

(2006) and Mai and Fleck (2009). This is a striking behaviour: when one of the bars of the lattice material is replaced by an actuator, the material is stiff against external loads when the actuator is not triggered. However, when the actuator is deployed the remaining structure can deform with minimal storage of internal energy. The 2D Kagome lattice and its 3D equivalent have particular promise along with tubes of walls made from a fully triangulated lattice.

Multi-functional applications of lattice materials require combinations of properties, such as high stiffness and toughness at low density. Some progress has been made on the development of theoretical bounds for cross-property correlations (eg between thermal conductivity and stiffness) as reviewed by Milton (2002). However, there remains a need for a prescription of the appropriate 2D or 3D lattice architectures that lead to the desired *combination* of properties in material property space.

The theoretical methods for obtaining bounds on linear properties such as modulus and thermal conductivity are now well developed. Progress has also been made on the development of bounds for strength, but not for toughness. Whilst strength is a bulk property, toughness is largely dictated by the weakest path of a crack. A wide range of toughening mechanisms exist in composites, including plasticity/internal friction, crack arrestors by crack tip blunting, distributed microcracking and controlled fragmentation. A research challenge remains to optimise lattice materials for high toughness, yet maintain a high stiffness and strength, with low density.

References

Ashby, M.F. (2010) "Materials selection in mechanical design", 4th edition, Butterworth Heinemann, Oxford, UK.

Ashby M.F. (1991) "On Material and Shape)" *Acta Materialia,* **39**, 1025-1039.

Ashby M.F., Evans A.G., Fleck N.A., Gibson L.J., Hutchinson J.W. and Wadley H.N.G. (2000). "Metal Foams: a Design Guide", Butterworth-Heinemann, Oxford, UK.

Calladine, C.R. (1978). "Buckminster Fuller's tensegrity structures and Clerk Maxwell's rules for construction of stiff frames", *Int. Solids Structs*. **14**, 161-172.

Cundy, H.M. and Rolett, A.P. (1961). "Mathetmatical models", Clarendon Press, Oxford.

Deshpande, V.S., Ashby, M.F. and Fleck, N.A. (2001). "Effective properties of the octet-truss lattice material". *J. Mech. Phys. Solids,* **49**, 1724-1769.

Deshpande, V.S., Ashby, M.F. and Fleck, N.A. (2001). "Foam topology: bending versus stretching dominated architectures". *Acta Materialia*, **49**, 1035-1040.

Fleck, N.A and Qiu, X. (2006). "The damage tolerance of elastic-brittle, two dimensional isotropic lattices" *J. Mech. Phys. Solids*. **55**, 562-588.

Frederickson, G.N. (1997). "Dissections: plane and fancy", Cambridge Univ. Press, Cambridge.

Gibson, L.J. and Ashby, M.F. (1997). "Cellular Solids. Structure and Properties" Cambridge University Pres, 2nd edn.

Hutchinson R.G. (2004). "Mechanics of lattice materials", Ph.D thesis, Cambridge University, UK.

Hutchinson, R.G. and Fleck, N. A. (2005). "Micro-architectured cellular solids – the hunt for statically determinate periodic trusses". *ZAMM*, **85(9),** 607-617.

Hutchinson, R.G. and Fleck, N.A. (2006). "The structural performance of the periodic truss". *J. Mech. Phys. Solids* **54**(4), 756-782.

Hyun, S. and Torquato, S. (2002). "Optimal and manufacturable two-dimensional Kagome-like cellular solids" *J. Mater. Res*, **17(1)**, 137-144.

Lockwood, E.H. and Macmillan R.H. (1978). "Geometric symmetry", Cambridge Univ. Press, Cambridge.

Mai, S.P. and Fleck, N.A. (2009). "Reticulated tubes: effective elastic properties and actuation response". *Proc. Roy. Soc. Lond.*, **465**, 685–708.

Milton, G. (2002). "The theory of composites", Cambridge University Press, Cambridge, UK.

Pellegrino, S. and Calladine, C.R. (1986). "Matrix analysis of statically and kinemantically indeterminate frameworks", *Int. Solids Structs*. **22(4)**, 409-428.

Quintana Alonso, I. and Fleck, N.A. (2009). "Compressive Response of a Sandwich Plate Containing a Cracked Diamond-Celled Lattice". *J. Mech. Phys. Solids*, **57** 1545–1567.

Romijn, N.E.R. and Fleck, N.A. (2007). "The fracture toughness of planar lattices: imperfection sensitivity". *J. Mech. Physics Solids*, **55**(12), 2538-2564.

Schmidt, I. and Fleck, N.A. (2001). "Ductile fracture of two-dimensional foams". *Int. J. Fracture*, **111**(4), 327-342.

Syozi, I. (1972). "Transformation of Ising models", in Phase transitions and critical phenomena, Domb, C. and Green, M.S. (eds). Academic Press.

Wadley, H.N.G., Fleck, N.A. and Evans, A.G. (2003). " Fabrication and structural performance of periodic cellular metal sandwich structures". *Comp. Sci. Tech.* **63**(16), 2331-2343.

Figure Captions

Fig. 1**.** A materials time-line. The scale is non-linear, with big steps at the bottom, small ones at the top. A star (*) indicates the date at which an element was first identified. Un-starred labels give the date at which the material became of practical importance.

Fig. 2. The progressive filling of material-property space over time (the charts list the date at the top left) – here the way the materials have been developed over time to meet demands on strength and density. Similar time-plots show the progressive filling of similar plots for all material properties.

Fig. 3. (a) Kagome lattice (b) triangular lattice, (c) hexagonal lattice.

Fig. 4. Venn diagram for selected 2D lattices

Fig. 5. Material property charts of E versus ρ and σ_Y versus ρ for engineering materials. Predictions for bending-dominated foams and stretching dominated lattices of CFRP and Aluminium superimposed. Lattices expand the occupied area of both charts.

Fig. 6. A hierarchical lattice on 2 length scales

Fig. 7. Boundary layer analysis: lattice material with a macroscopic crack under *K*-control. The joint displacements and rotations associated to a *K*-field are prescribed on the outer boundary.

Fig. 8. The predicted mode I fracture toughness K_{IC} plotted as a function of relative density $\bar{\rho} \propto t/\ell$, for the three isotropic lattices: hexagonal, triangular and Kagome.

Fig. 9. Predictions of the scaling of the fracture toughness of the Kagome lattice with relative density for three choices of the length scale ratio ℓ / a_0 and $\bar{\rho}_0 = 0.3$.

Fig. 10. A plot of fracture toughness, K_{IC}, against density ρ for engineering materials. It shows how the fracture toughness of a zirconia Kagome lattice is predicted to evolve with density. At low densities the lattice is far tougher than foams with a bending dominated architecture.

Fig. 11. The damage tolerance of a lattice material and the parent solid.

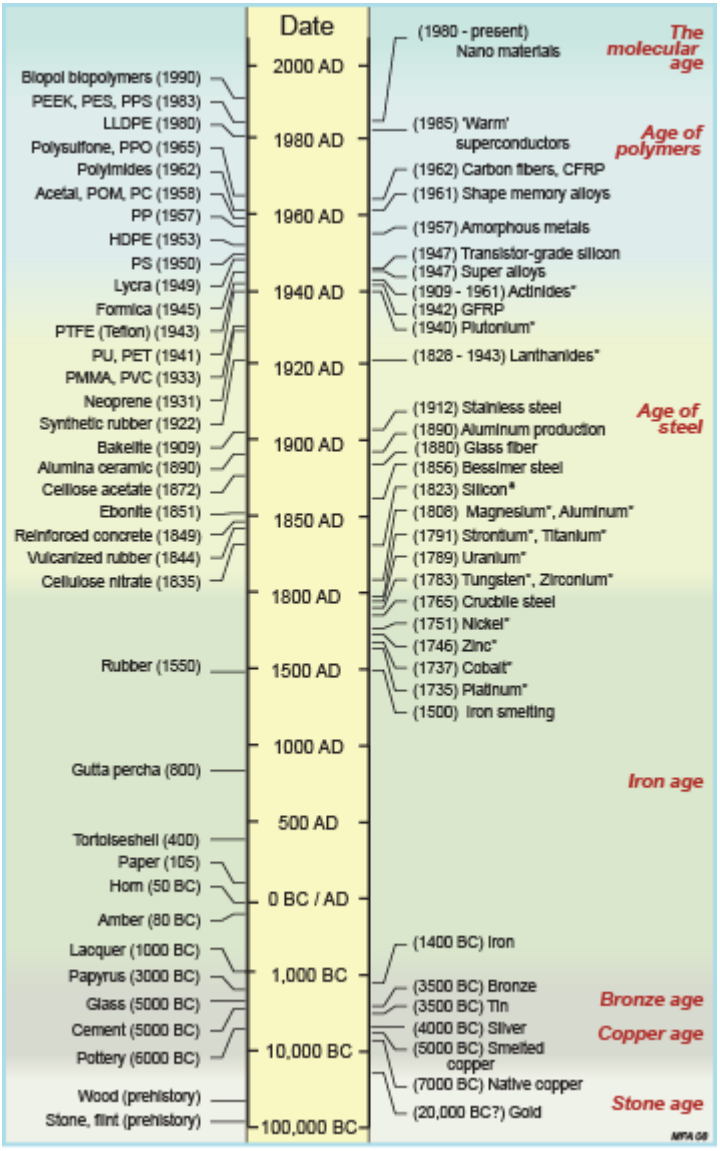

Fig. 1. A materials time-line. The scale is non-linear, with big steps at the bottom, small ones at the top. A star (*) indicates the date at which an element was first identified. Un-starred labels give the date at which the material became of practical importance.

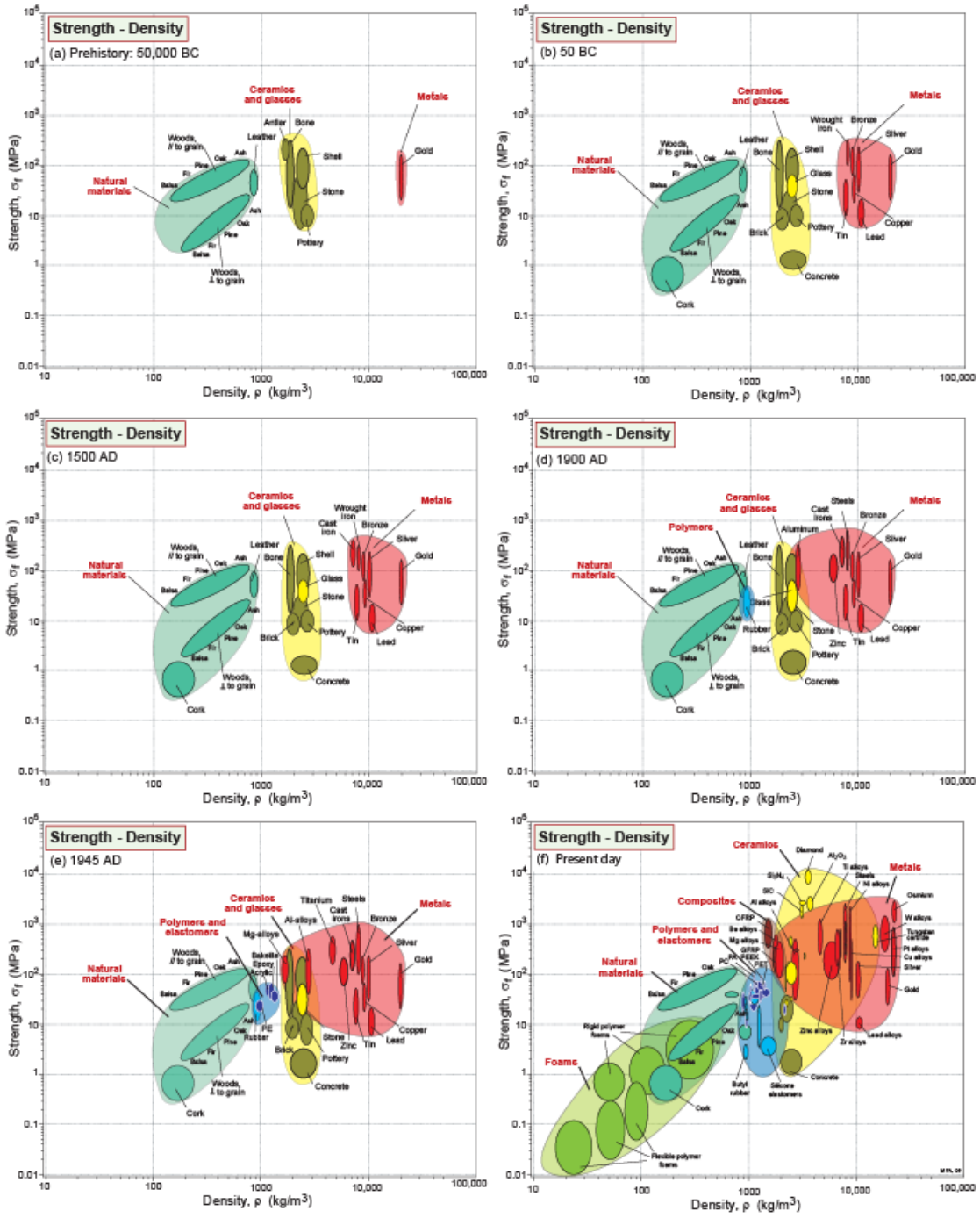

Fig. 2. The progressive filling of material-property space over time (the charts list the date at the top left) – here the way the materials have been developed over time to meet demands on strength and density. Similar time-plots show the progressive filling of similar plots for all material properties.

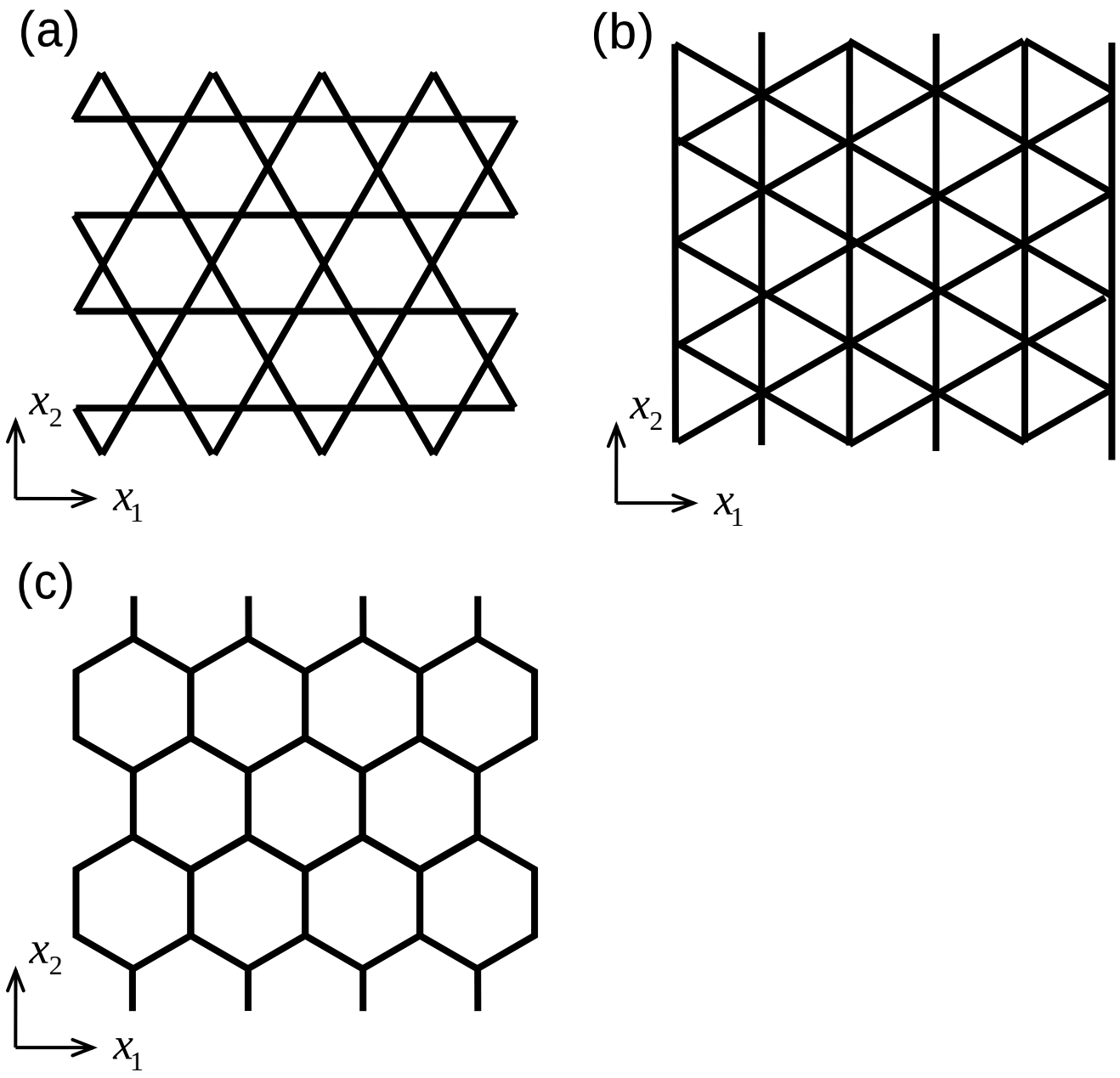

Fig. 3. (a) Kagome lattice (b) triangular lattice, (c) hexagonal lattice.

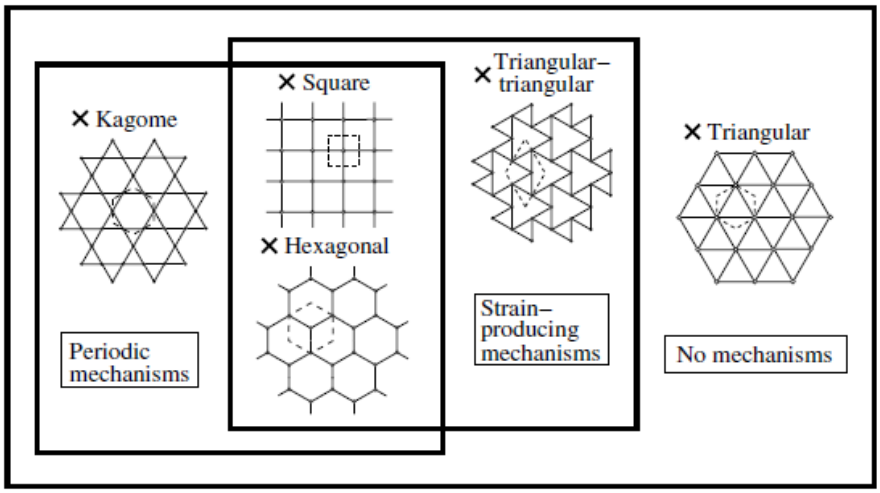

Fig. 4. Venn diagram for selected 2D lattices.

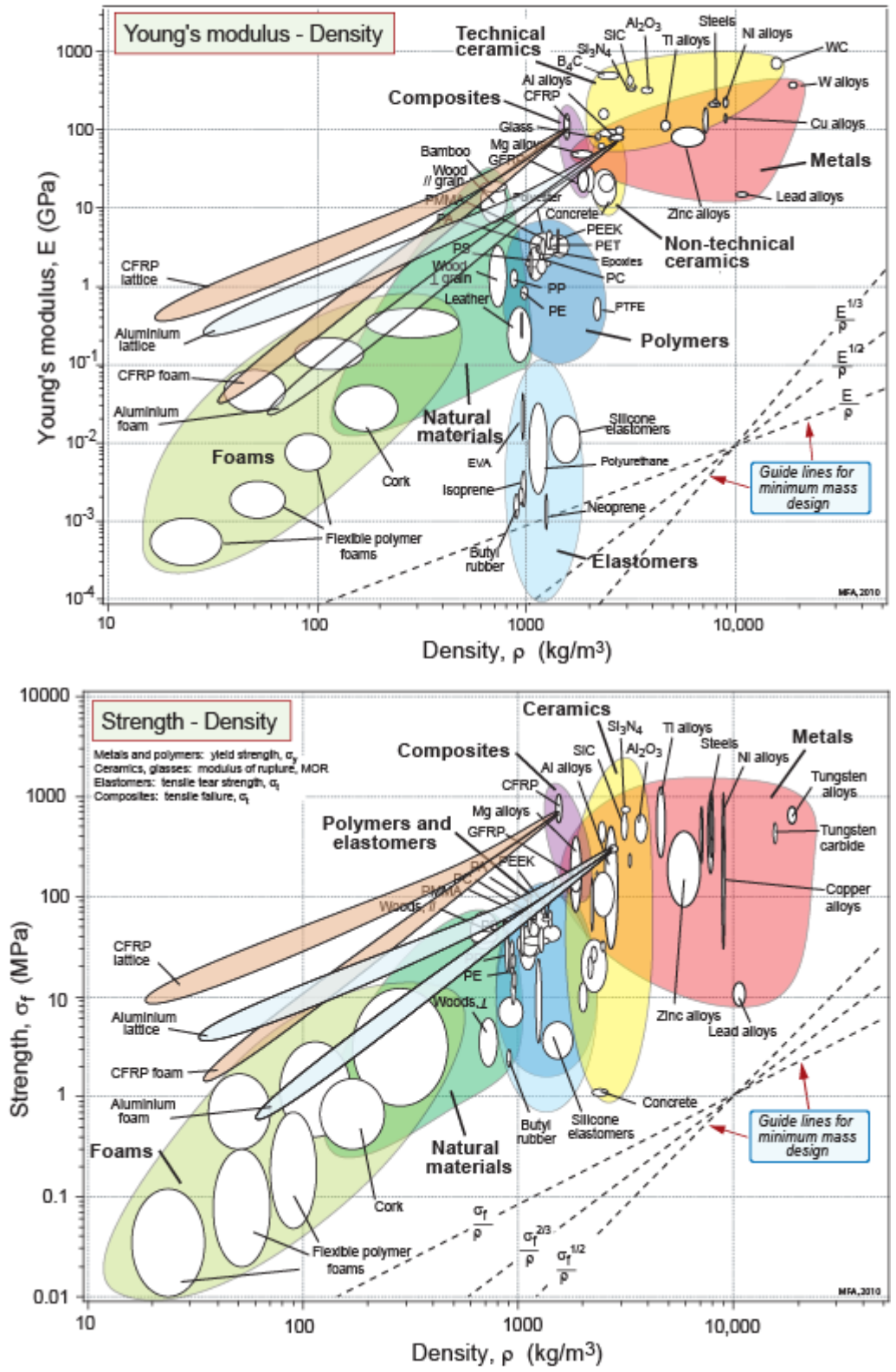

Fig. 5. Material property charts of E versus ρ and σ_Y versus ρ for engineering materials. Predictions for bending-dominated foams and stretching dominated lattices of CFRP and Aluminium superimposed. Lattices expand the occupied area of both charts.

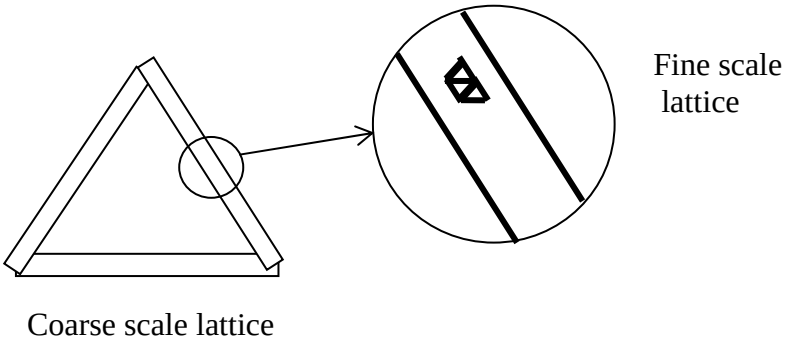

Fig. 6. A hierarchical lattice on 2 length scales

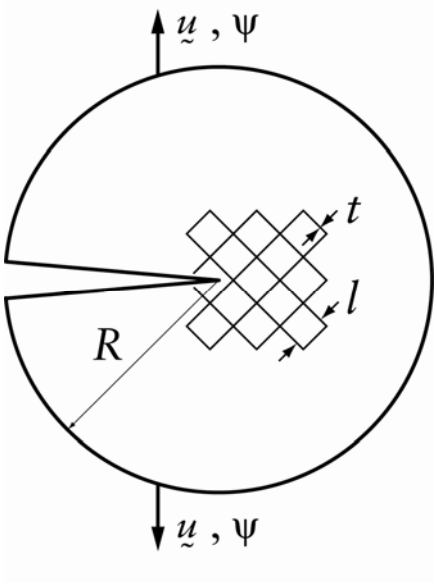

Fig. 7. Boundary layer analysis: lattice material with a macroscopic crack under *K*-control. The joint displacements and rotations associated to a *K*-field are prescribed on the outer boundary.

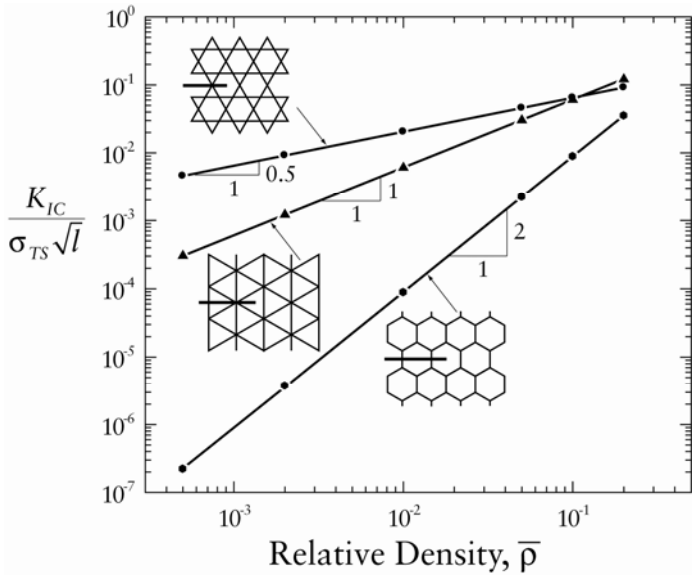

Fig. 8. The predicted mode I fracture toughness K_{IC} plotted as a function of relative density $\bar{\rho} \propto t / \ell$, for the three isotropic lattices: hexagonal, triangular and Kagome.

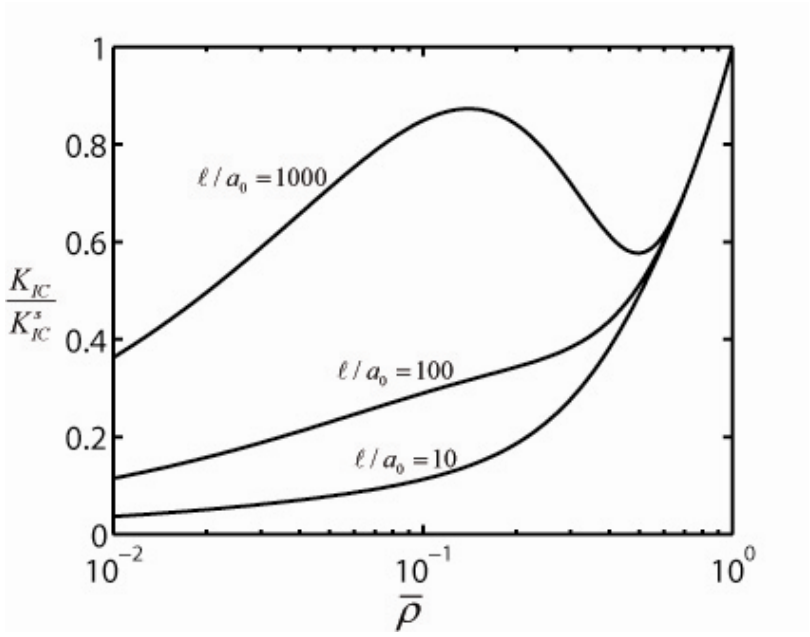

Fig. 9. Predictions of the scaling of the fracture toughness of the Kagome lattice with relative density for three choices of the length scale ratio ℓ / a_0 and $\bar{\rho}_0 = 0.3$.

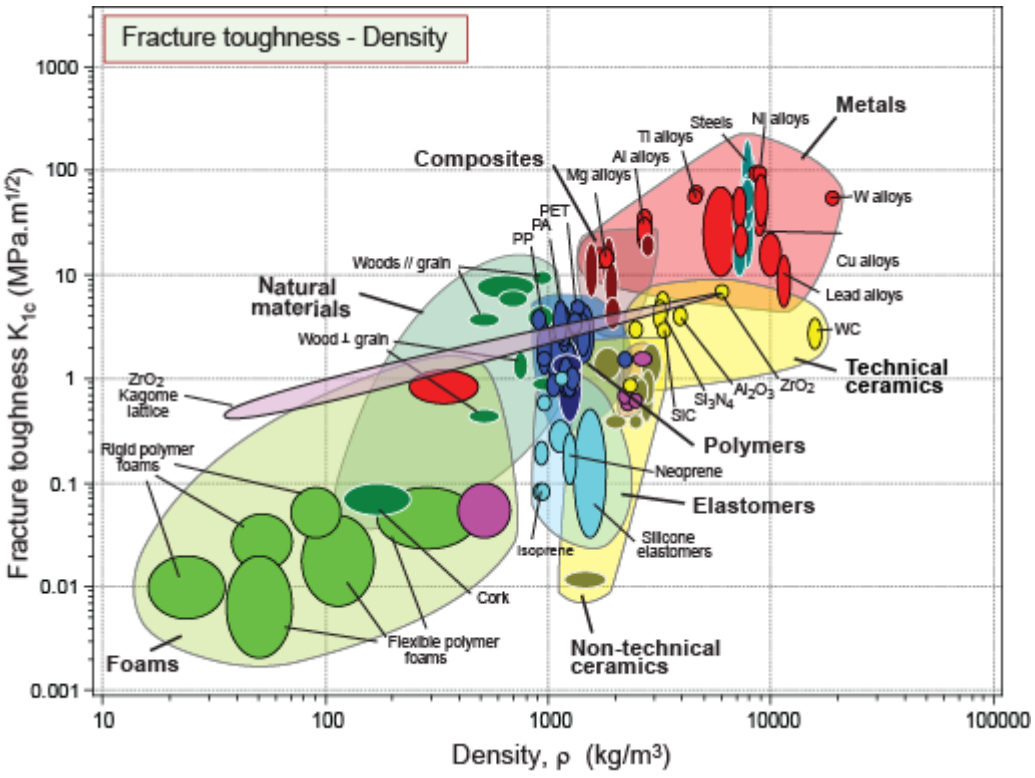

Fig. 10. A plot of fracture toughness, K_{IC}, against density ρ for engineering materials. It shows how the fracture toughness of a zirconia Kagome lattice is predicted to evolve with density. At low densities the lattice is far tougher than foams with a bending dominated architecture.

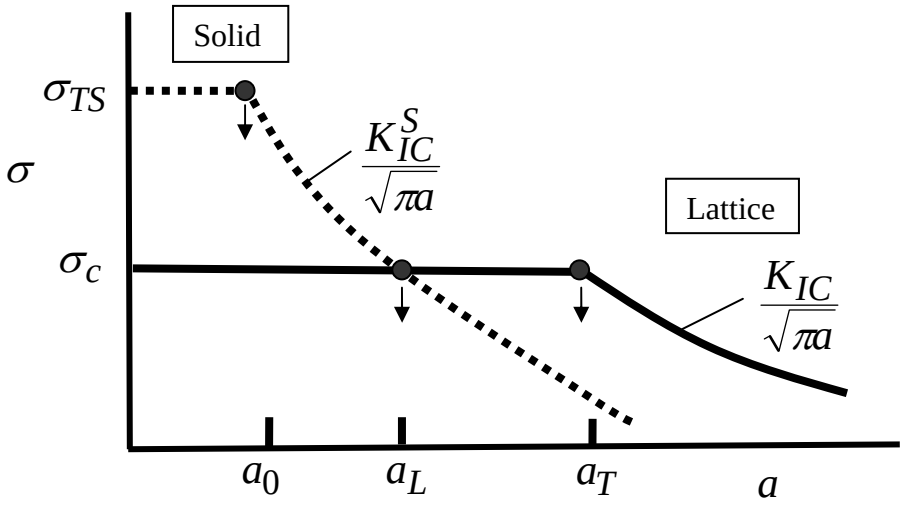

Fig. 11. The damage tolerance of a lattice material and the parent solid.